CIRP Annals - Manufacturing Technology 61 (2012) 547–550

Contents lists available at SciVerse ScienceDirect

CIRP Annals - Manufacturing Technology

journal homepage: http://ees.elsevier.com/cirp/default.asp

Prediction of machining induced residual stresses in turning of titanium and nickel based alloys with experiments and finite element simulations

T. Özel (2)*, D. Ulutan

Manufacturing & Automation Research Laboratory, Department of Industrial and Systems Engineering, Rutgers University, NJ, USA

ARTICLE INFO

Keywords:
Turning
Residual stress
Finite element method

ABSTRACT

Titanium and nickel alloys represent a significant metal portion of the aircraft structural and engine components and the residual stresses induced by machining are very critical due to safety and sustainability concerns. This paper presents experimental investigations and finite element simulations on turning of Ti–6Al–4V titanium alloy and IN100 nickel based alloy with uncoated and TiAlN coated tools. Face turning of Ti–6Al–4V and IN100 using uncoated tools with various edge radii and TiAlN coated carbide tools is conducted; and residual stresses are measured in radial and circumferential directions using X-ray diffraction technique. 3-D finite element (FE) modeling is utilized to predict forces and machining induced stress fields. The feasibility and limitations of predicting machining induced residual stresses by using viscoplastic finite element simulations and temperature-dependent flow softening constitutive material modeling are investigated. A friction determination method is utilized to identify friction coefficients in presence of tool edge radius. The predicted stress fields are compared against measured residual stresses. Effect of tool edge radius and coating on the predicted stress profiles is also investigated. The results are found useful in predicting machining induced surface integrity that is critical to determine the fatigue life of nickel and titanium alloy components.

1. Introduction

Titanium and nickel alloys are difficult-to-machine materials with considerable manufacturing problems such as machining induced surface integrity and residual stresses [1]. Titanium alloys, specifically Ti–6Al–4V, are used in many industries including aerospace, automotive and medical device and offer favorable mechanical characteristics such as high strength-to-weight ratio, toughness, superb corrosion resistance and bio-compatibility. Nickel-based super alloys are often used in mission critical components such as in aircraft/industrial gas turbine engines. Particularly, IN100 nickel-based alloy manufactured via powder metallurgy route is rated as extremely difficult-to-machine due to the high toughness and work hardening behavior in which a work hardened layer forms in response to the machining induced thermal and plastic deformations on the subsurface [2].

Most such structural components are finish-machined. When the thermo-mechanical load on the workpiece material is released, the residual stresses that remain in the material after unloading, which are considered to be mainly due to machining-induced plastic work at the subsurface and thermal effects at the surface due to friction and tool wear, are revealed [3]. In case of high tensile stress, which is considered detrimental to the fatigue life of the component, the machined component undergoes costly surface treatment operations to create a compressively stressed surface. Therefore, when such components in the industry are manufactured with the objective of reaching high reliability levels, machining-induced surface integrity becomes one of the most relevant parameters for the fatigue life of these components. In general, machining-induced residual stresses are more tensile at the surface of the workpiece and become compressive as the depth in the workpiece increases to around 50 μm [2–4]. In addition, an increase in feed rate makes the residual stresses more tensile at the surface and more compressive in the peak compressive depth, especially at higher cutting speeds, where the peak residual stresses might become less compressive with increasing feed in lower cutting speeds [3–5]. In the presence of tool flank wear, the residual stress profiles change and become more tensile due to increased heat generation and related thermal effects. For example, the effect of flank wear on residual stress (in axial direction) is investigated by Chen et al. [6] for Ti–6Al–4V and Sharman et al. [7] for IN718. Circumferential or hoop stresses (in the direction of cutting velocity vector) are mainly compressive on the machined surface when using a fresh unworn tool. However, circumferential stresses turn tensile when cutting with a worn tool or in presence of tool flank contact. This is consistent with machining both Ti–6Al–4V titanium alloy and IN718 nickel alloy. Tool material also affects residual stress formation. Outeiro et al. [8] reported higher tensile surface residual stress generation when machining with the uncoated tungsten carbide (WC/Co) when compared to TiAlN coated tungsten carbide tool in machining IN718 nickel based alloy. Although some influence of cutting edge geometry on machining has been shown [5], its effect on machining induced residual stresses has not been fully explored.

In this research, uncoated tools with various edge radii and TiAlN coated tungsten carbide inserts (WC/Co) have been tested to explore the effects of tool geometry and coatings on machining

* Corresponding author.

0007-8506/$ – see front matter © 2012 CIRP.
http://dx.doi.org/10.1016/j.cirp.2012.03.100

induced residual stress in Ti–6Al–4V titanium and IN100 nickel based alloy. Finite element (FE) simulations are utilized in predicting machining induced stresses with experimental comparisons. Three dimensional FE simulations have been designed and conducted to predict forces, temperatures and stress fields to investigate the effects of tool micro-geometry and coatings in machining of Ti–6Al–4V and IN100.

2. Experimental work

Titanium alloy material, annealed Ti–6Al–4V, has been obtained as cylindrical billets with 100 mm diameter in annealed conditions with 36 HRC hardness. Nickel based alloy material used in this study, IN100, is manufactured via powder metallurgy route with a chemical composition of 18.3% Co, 12.3% Cr, 4.9% Al, 4.3% Ti, 3.3% Mo, 0.7% V, 0.1% Fe, 0.06% C, 0.02% B, 0.02% Zr and Ni balance. This material was isostatically pressed and cylindrical billets were formed. Disks with 113 mm diameter were cut from the billet with wire electrical discharge machining (WEDM) process. Face turning of annealed Ti–6Al–4V titanium alloy and IN100 nickel based alloy disks was performed by using TPG432 type insert geometry (insert nose radius of r_ε = 0.8 mm and relief angle of $\alpha = 11^\circ$) in a rigid CNC turning lathe under dry machining conditions as shown in Fig. 1. Tool edge radii were measured as $r_\beta = 5 \pm 0.5$ μm for sharp uncoated tungsten carbide (WC/Co) and $r_\beta = 10 \pm 0.7$ μm for TiAlN coated WC/Co respectively. In addition, uncoated sharp tools were edge prepared using abrasive brushing technique to have edge radii of $r_\beta = 10 \pm 0.7$ μm and $r_\beta = 25 \pm 1.0$ μm. The inserts were mounted in a CTFPR-164C right hand tool holder that provided 0° lead, 0° side rake, and −5° back rake angles. Two or three tracks have been machined on the face using different cutting conditions. After each face turning test, disks with approximately 3 mm thickness have been sliced out of the cylindrical workpiece.

In the experiments, WC/Co inserts with three different edge radii of $r_\beta \cong 5$, 10, and 25 μm, and TiAlN coated WC/Co inserts with edge radius of $r_\beta \cong 10$ μm have been tested in face turning of Ti–6Al–4V and IN100 disks. Two cutting speeds of v_c = 12 m/min and 24 m/min, a depth of cut of a_p = 1 mm and a constant feed of f = 0.05 mm/rev for IN100 nickel based alloy and a depth of cut of a_p = 2 mm, two cutting speeds of 55 m/min and 90 m/min and two feeds of f = 0.05 mm/rev and 0.1 mm/rev for Ti–6Al–4V were selected as cutting conditions. The cutting forces were measured with a force dynamometer mounted on the turret disk of the CNC lathe. The averages of the measured forces for each insert are shown in Fig. 2. In face turning of IN100, lowest forces are obtained using TiAlN coated WC/Co tool at the lower cutting speed (v_c = 12 m/min). But the performance of uncoated WC/Co ($r_\beta \cong 25$ μm) tool became the same as TiAlN coated at the higher cutting speed (v_c = 24 m/min). In machining Ti–6Al–4V at both cutting speeds, uncoated WC/Co ($r_\beta \cong 25$ μm) tool resulted in lower forces regardless of the feed rate.

3. Residual stress measurements

After all the machining process was completed in Ti–6Al–4V alloy disks, residual stresses were measured using X-ray diffraction technique on Bruker HiStar unit using Cu-K_α radiation (λ = 1.54 Å) at 20 kV, 2 mA to acquire {1 1 4} and {2 1 3} diffraction peaks or lines at 2θ angles of about 115° and 140° respectively using a spot

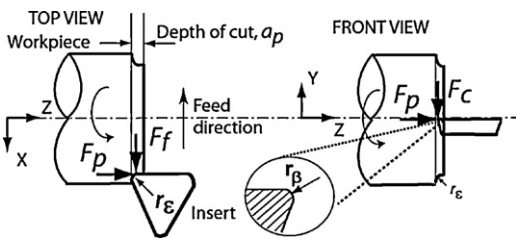

Fig. 1. Configuration of face turning experiments.

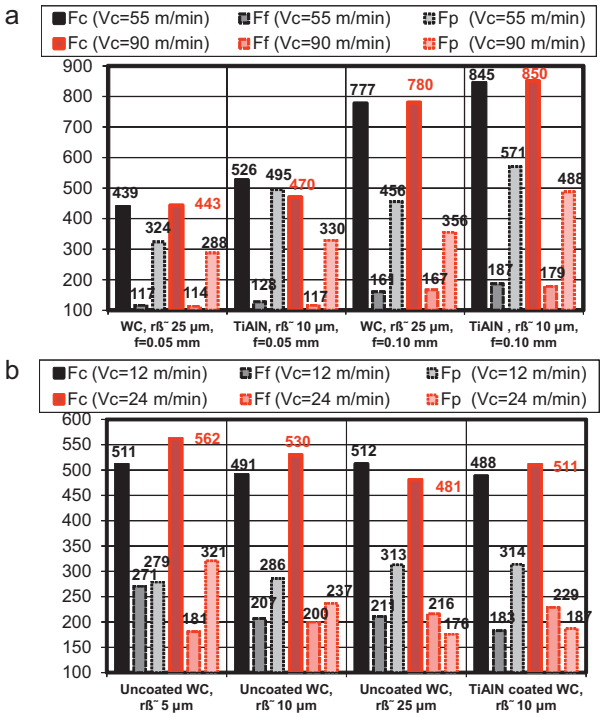

Fig. 2. Forces measured in face turning of Ti–6Al–4V (a) and IN100 (b).

size of 1 mm collimated from 2 mm beam by using a tungsten filament. In order to prevent the detection of banding created due to presence of Cu within the disks, a nickel foil was used to filter the detected radiation beams. This banding, when not filtered, hinders the accuracy of measurements. The residual stresses through the depth profiles of the disks were measured by chemically etching successive layers of material to a depth in excess of 100 μm using a titanium etchant reagent (8–30% HFl and 70–92% H_2O). Residual stresses on IN100 disks were measured using X-ray diffraction technique on Proto iXRD unit Mn–Cu-K_α radiation (λ = 2.1 Å) at 17 kV, 4 mA to acquire {3 1 1} diffraction peaks or lines at 2θ angles of about 155° using a spot size of 1 mm × 2 mm beam. Similarly, residual stresses and depth profiles were measured by removing successive layers of material to a depth in excess of 100 μm by electropolishing. In-plane surface stress measurements were performed at selective positions from inner and outer radial positions along the tracks on the disks that were machined with face turning.

3.1. 3D finite element simulations

Recently, finite element simulation models of chip formation begin to enable prediction of machining-induced residual stresses and optimization of tool micro-geometry and machining parameters without running costly experimentation [9]. However, 3D FE simulation models still suffer from not only numerical convergence problems (elastic–viscoplastic deformations) but also uncertainty associated with calculated output variables. For the purpose of identifying prediction accuracy, 3D finite element models are developed using updated Lagrangian software (DEFORM-3D) in which chip separation from workpiece is achieved with continuous remeshing. The simulations included a workpiece as viscoplastic with a mesh containing 1.5×10^5 quadrilateral elements. Tool is modelled as rigid with a mesh containing into 1.0×10^5 elements. The workpiece is represented by a curved model, a 4° segment of disk surface, with the disk diameter used in experimental conditions. The bottom surface of this workpiece is fixed in all directions. A small segment around the corner radius area of the cutting insert (r_ε = 0.8 mm with 11° relief angle) is modelled as a rigid body which moves at the specified cutting speed [9]. A very fine mesh density is defined at

Table 1
Mechanical and thermo-physical properties of work and tool materials used in FE simulations.

	Ti–6Al–4V	IN100	WC/Co	(Ti,Al)N
$E(T)$	$0.7412T+113{,}375$	$-61{,}000T+278{,}000$	5.6×10^5	6.0×10^5
$\alpha(T)$	$3.10^{-9}T+7.10^{-6}$	$10^{-5}e^{0.0849T}$	4.7×10^{-6}	9.4×10^{-6}
$\lambda(T)$	$7.039e^{0.0011T}$	$10.409e^{0.0903T}$	55	$0.0081T+11.95$
$c_p(T)$	$2.24e^{0.0007T}$	$418.63e^{0.0433T}$	$0.0005T+2.07$	$0.0003T+0.57$

Table 2
Material model parameters used in FE simulations.

Alloy	A (MPa)	B (MPa)	n	C	m	D	p	r	s
Ti–6Al–4V	1000	625	0.55	0.029	0.995	0.48	0	1.2	2.7
IN100	1350	1750	0.65	0.017	1.3	0.6	0	1.0	5.0

the tip of the tool and at the cutting zone to obtain fine process output distributions. In average, minimum element size for the workpiece and tool mesh was set to 0.005 mm and 0.015 mm respectively. Thermal boundary conditions are defined accordingly in order to allow heat transfer from workpiece to cutting tool. The heat conduction coefficient (h) is taken as 100 kW/m^2/°C to allow rapid temperature rise in the tool. Mechanical and thermo-physical properties of work material are defined as temperature (T) dependent. Temperature-dependent (T in °C) modulus of elasticity (E in MPa), thermal expansion (α in 1/°C), thermal conductivity (λ in W/m/°C), and heat capacity (c_p in N/mm^2/°C) are given in Table 1.

In the 3D FE model, friction at the tool–chip contact was handled using a hybrid model: (i) a shear friction region ($m=\tau/k$ where τ is shear stress and k is shear flow stress) around the tool edge radius curvature ($m=0.9$) and (ii) a sliding region along the rest of the rake face ($0.6\le\mu\le0.8$ for as the friction coefficients).

In FE simulations, a constitutive material model is required to relate the flow stress to strain, strain rate and temperature, which is often obtained from Split-Hopkinson pressure bar (SHPB) tests performed under various strain rates and temperatures. Dynamic material behavior for Ti–6Al–4V titanium alloy has been widely published in literature and a phenomenon known as strain (flow) softening is observed [9]. On the other hand, dynamic material behavior data for nickel-based alloys do not appear in the published literature with a very few exceptions. Zhang et al. [10] investigated strain-rate sensitivity of IN718 at high temperatures and also observed flow softening behavior. Therefore, in this work, a modified material model given in Eq. (1) is used that includes the temperature-dependent flow softening effect in addition to strain and strain rate hardening and thermal softening effects [11].

$$\sigma=[A+B\varepsilon^n]\left[1+C\ln\frac{\dot\varepsilon}{\dot\varepsilon_o}\right]\left[1-\left(\frac{T-T_o}{T_m-T_o}\right)^m\right]\times\left[D+(1-D)\left[\tanh\left(\frac{1}{(\varepsilon+p)^r}\right)\right]^s\right]$$

where σ is flow stress, ε is true strain, $\dot\varepsilon$ is true strain rate, $\dot\varepsilon_o$ is reference true strain, and T, T_m, T_o are work, material melting and ambient temperatures respectively. The set of model parameters used in the model for Ti–6Al–4V alloy and IN100 nickel based alloy are given in Table 2. The melting temperature for Ti–6Al–4V and IN100 used is T_m = 1604 °C and 1490 °C respectively.

All simulations were run at the same experimental conditions. In Tables 3 and 4, mean and standard deviation of the simulated forces (F_c, cutting force; F_p, thrust force; and F_f, feed force) as compared with experimental ones are given. Mean and standard deviation values for simulated tool and work temperatures are also given in the same tables. For IN100, cutting forces are in close agreements with about 5% prediction error. Thrust and feed force predictions showed an error of 1–15%. For Ti–6Al–4V, cutting forces showed about 4% prediction error. Thrust and feed force predictions showed an error of 20–45%. The temperatures (>600 °C for IN100 and >550 °C for Ti–6Al–4V) in the cutting zone can create significant thermal strain contributing to the machining induced strain and stress fields.

4. Prediction of machining induced residual stress

FE simulation predictions in machining Ti–6Al–4V alloy indicated that circumferential residual stresses at the surface increased with increasing cutting speed, while the tool coating/edge radius change did not affect these values (Fig. 3). Compressive peak residual stresses in circumferential direction were not significant for all tests, but they all showed this peak around 80 μm at approximately −100 MPa. This peak was slightly more compressive with the coated tool compared to the uncoated tool. In the radial direction, all tests showed compressive residual stresses both at the surface and deep into the material. They all occurred at

Table 3
Summary of FE simulation on IN100 force and temperature predictions (f = 0.05 mm/rev and v_c = 24 m/min).

Tool type	F_c Sim (N)	F_c Exp (N)	F_p Sim (N)	F_p Exp (N)	F_f Sim (N)	F_f Exp (N)	*Temp* Tool (°C)	*Temp* Chip (°C)
WC/Co $r_\beta\cong5$ μm	592 ± 38	562 ± 35	302 ± 21	321 ± 31	196 ± 24	181 ± 10	607 ± 51	645 ± 44
WC/Co $r_\beta\cong10$ μm	511 ± 44	530 ± 37	248 ± 36	237 ± 31	182 ± 22	200 ± 9	556 ± 63	602 ± 62
WC/Co $r_\beta\cong25$ μm	513 ± 49	481 ± 24	203 ± 33	176 ± 26	242 ± 24	216 ± 9	590 ± 64	637 ± 57
TiAlN $r_\beta\cong10$ μm	506 ± 41	511 ± 27	187 ± 18	187 ± 38	232 ± 31	229 ± 24	580 ± 57	623 ± 52

Table 4
Summary of FE simulation on Ti–6Al–4V force and temperature predictions (f = 0.1 mm/rev).

Tool type	F_c Sim (N)	F_c Exp (N)	F_p Sim (N)	F_p Exp (N)	F_f Sim (N)	F_f Exp (N)	*Temp* Tool (°C)	*Temp* Chip (°C)
WC/Co v_c = 55 m/min	748 ± 21	777 ± 20	364 ± 18	456 ± 47	202 ± 13	161 ± 16	485 ± 52	564 ± 46
TiAlN v_c = 55 m/min	854 ± 39	845 ± 29	347 ± 22	571 ± 47	96 ± 11	187 ± 15	503 ± 66	587 ± 53
WC/Co v_c = 90 m/min	759 ± 33	780 ± 24	307 ± 32	356 ± 48	188 ± 19	167 ± 24	596 ± 56	643 ± 75
TiAlN v_c = 90 m/min	840 ± 26	850 ± 33	318 ± 17	488 ± 51	77 ± 12	179 ± 24	614 ± 47	667 ± 58

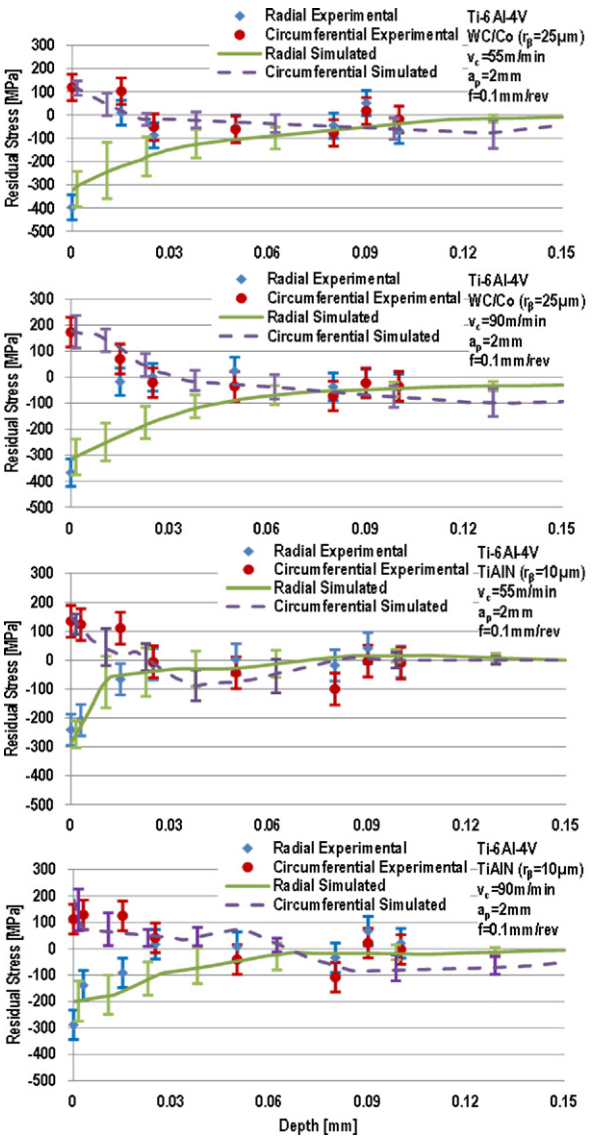

Fig. 3. Comparison of residual stresses in face turning of Ti–6Al–4V.

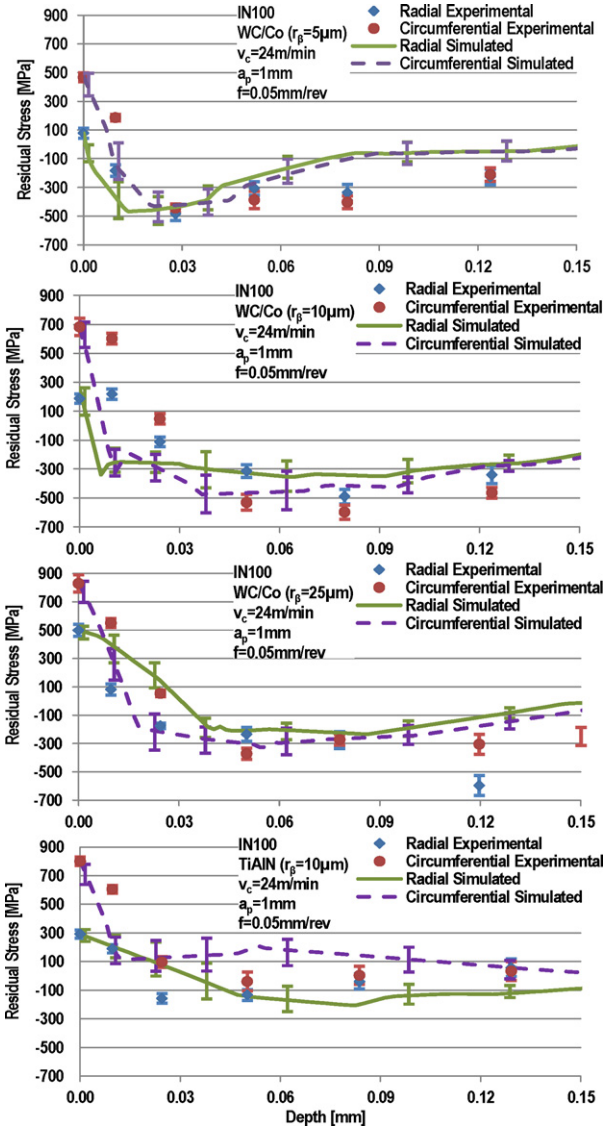

Fig. 4. Comparison of residual stresses in face turning of IN100.

approximately −250 to −400 MPa. The prediction accuracy for the simulations was found better for the circumferential residual stresses rather than the radial direction which was found inferior. In IN100, prediction accuracy of the simulations was better in both circumferential and radial directions (Fig. 4). For both circumferential and radial directions, surface tensile residual stresses showed an increase with increasing cutting edge radius, and the coated tool showed a slightly less tensile residual stress at the surface than the 25 μm edge radius tool. Compressive peak residual stresses varied from −400 to −600 MPa for the uncoated tools and were not significant for the TiAlN coated tool. Measurement and prediction uncertainty in residual stress findings are indicated with standard deviation bars in both Figs. 3 and 4.

5. Conclusions

In this study, 3D FE simulations to predict machining induced residual stresses in Ti–6Al–4V and IN100 alloys are utilized. Results are compared with experiments. It is concluded that predicted residual stresses are influenced by the tool micro-geometry as they become more compressive with increased edge radius but more tensile at the surface when coated.

Acknowledgment

The authors gratefully acknowledge the support by the National Science Foundation (grant number CMMI-1130780).

References

[1] Jawahir IS, Brinksmeier E, M'Saoubi R, Aspinwall DK, Outeiro JC, Meyer D, Umbrello D, Jayal AD (2011) Surface Integrity in Material Removal Processes: Recent Advances. *CIRP Annals – Manufacturing Technology* 60(2):603–626.
[2] Ulutan D, Özel T (2011) Machining Induced Surface Integrity in Titanium and Nickel Alloys: A Review. *International Journal of Machine Tools & Manufacture* 51:250–280.
[3] Li W, Withers PJ, Preuss M, Shackleton J, Andrews P (2011) Depth and Lateral Variation of Machining-Induced Residual Stress for A Nickel Base Superalloy. *Materials Science Forum* 681:332–339.
[4] Che-Haron CH, Jawaid A (2005) The Effect of Machining on Surface Integrity of Titanium. *Journal of Materials Processing Technology* 166:188–192.
[5] Pawade RS, Joshi SS, Brahmankar PK (2008) Effect of Machining Parameters and Cutting Edge Geometry on Surface Integrity of High-Speed Turned Inconel 718. *International Journal of Machine Tools & Manufacture* 48:15–28.
[6] Chen L, El-Wardany TI, Harris WC (2004) Modeling the Effects of Flank Wear Land and Chip Formation on Residual Stresses. *CIRP Annals – Manufacturing Technology* 53(1):95–98.
[7] Sharman ARC, Hughes JI, Ridgway K (2006) An Analysis of the Residual Stresses Generated in Inconel 718 When Turning. *Journal of Materials Processing Technology* 173:359–367.
[8] Outeiro JC, Pina JC, M'Saoubi R, Pusavec F, Jawahir IS (2008) Analysis of Residual Stresses Induced by Dry Turning of Difficult-To-Machine Materials. *CIRP Annals – Manufacturing Technology* 57(1):77–80.
[9] Özel T, Sima M, Srivastava AK, Kaftanoglu K (2010) Investigations on the Effects of Multi-Layered Coated Inserts in Machining Ti–6Al–4V Alloy with Experiments and Finite Element Simulations. *CIRP Annals – Manufacturing Technology* 59(2):77–82.
[10] Zhang JM, Gao ZY, Zhuang JY, Zhong ZY, Janschek P (1997) Strain-Rate Hardening Behavior of Superalloy IN718. *Journal of Materials Processing Technology* 70:252–257.
[11] Ulutan D, Sima M, Özel T (2011) Prediction of Machining Induced Surface Integrity using Elastic–Viscoplastic Simulations and Temperature-Dependent Flow Softening Material Models in Titanium and Nickel-Based Alloys. *Advanced Materials Research* 223:401–410.